High-energy resummation for Higgs boson plus jets production

Andreas Maier[a,*]

[a]*Deutsches Elektronen-Synchrotron DESY, Platanenallee 6, 15738 Zeuthen, Germany*

E-mail: andreas.martin.maier@desy.de

At high energies, fixed-order predictions for the production of a Higgs boson together with one or more jets suffer from large logarithms in invariant masses over transverse momenta. We resum these high-energy logarithms to all orders within the *High Energy Jets* (HEJ) framework, retaining the exact dependence on the top-quark mass. We compare our predictions to ATLAS and CMS measurements at 8 and 13 TeV.

---

[*]Speaker

1. Introduction

One of the central aims of the LHC physics programme is to explore the Higgs sector through precision measurements, and it is one of the biggest current challenges in high-energy physics to match the precision of these measurements on the theory side. On the one hand, higher-order corrections in processes involving Higgs bosons tend to be numerically large (see e.g. [1]) and computations at high perturbative orders are needed to meet the precision goals. On the other hand, the dominant production channel through gluon fusion is loop-induced, which quickly renders exact calculations of loop corrections prohibitively difficult. These difficulties can be alleviated by resorting to kinematic approximations. In addition to simplifying fixed-order computations, expansions exploiting scale hierarchies can be used to resum the dominant corrections to all orders in perturbation theory.

Among the different Higgs boson production channels, weak boson fusion is of particular interest, allowing a direct measurement of the Higgs couplings to W and Z bosons. Correspondingly, the contribution to Higgs boson plus dijet production from this channel has been computed to very high orders, namely to next-to-next-to-next-to leading order (N^{3}LO) in QCD [2–4], including non-factorising contributions [5], and to next-to-leading order (NLO) in the electroweak sector [6]. However, other production channels for the same process are much less well known. In particular, the dominant gluon-fusion channel is only known exactly at leading order (LO) [7]. To suppress the gluon-fusion contribution one therefore applies weak boson fusion cuts requiring a large invariant mass and rapidity separation between the two hardest jets.

The kinematic requirements imposed by weak boson fusion cuts provide a strong motivation to study Higgs boson plus jets production via gluon fusion in the high-energy limit, defined by large rapidity separations between the outgoing particles and the absence of strong hierarchies in transverse momenta. Equivalently, the high-energy regime is characterised by invariant masses that are large compared to all transverse scale. In the following, we discuss all-order predictions for the gluon-fusion production of a Higgs boson together with one or more jets at high energies. In order to obtain a realistic description, we employ the *High Energy Jets* [8–10] framework, matching to fixed-order predictions at leading order.

2. Higgs boson plus jets production at high energies

2.1 High-energy scaling

To identify the leading high-energy contributions, we order the n final-state particles with momenta $p_1, \ldots, p_n$ by their rapidities $y_1, \ldots, y_n$, such that $y_1 < \cdots < y_n$. The behaviour of the amplitude in the high-energy limit is then determined by Regge scaling [11], namely

$$\mathcal{M} \sim m_{12}^{\alpha_1} \ldots m_{n-1n}^{\alpha_{n-1}}, \tag{1}$$

where m_{ii+1} is the invariant mass between the outgoing particles i and $i+1$ and α_i the largest spin that can be exchanged between these two particles. In QCD, the amplitude is therefore dominated by those configurations that allow the maximum number of t-channel gluons. It should be emphasised that this criterion is gauge-invariant. An example for a leading and a subleading configuration is shown in figure 1.
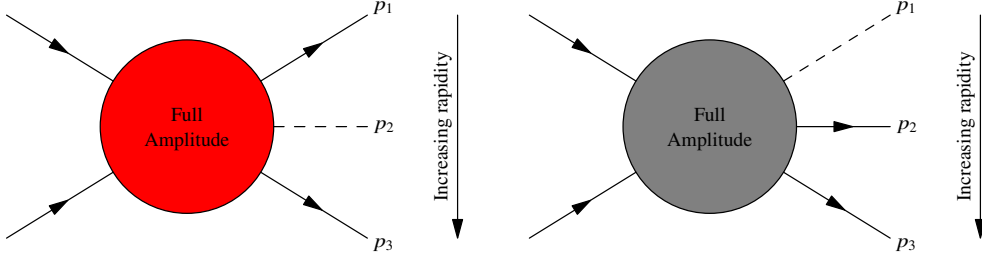
Figure 1: Scaling behaviour of two sample configurations in Higgs boson plus dijet production. The configuration on the left allows the maximum of two t-channel gluon exchanges and is therefore leading in the high-energy limit. In the subleading configuration on the right there is at most one t-channel gluon exchange.

2.2 Higgs boson plus jets production within *High Energy Jets*

High Energy Jets (HEJ) is a framework for the all-order resummation of high-energy logarithms of the form $\left(\alpha_s \ln \frac{m_{ij}}{p_\perp}\right)^N$. Currently, leading-logarithmic (LL) resummation is implemented for all leading configurations. In addition, next-to-leading-logarithmic (NLL) contributions originating from selected subleading configurations are included as detailed below. Only minimal approximations are applied such that exact tree-level gauge invariance is preserved. Indeed, for simple processes the matrix elements are tree-level exact for leading high-energy configurations. There are no approximations at the phase-space level, apart from the restriction to leading and selected subleading configurations. The framework allows for fully flexible Monte Carlo event generation including realistic cuts.

2.2.1 Matrix elements
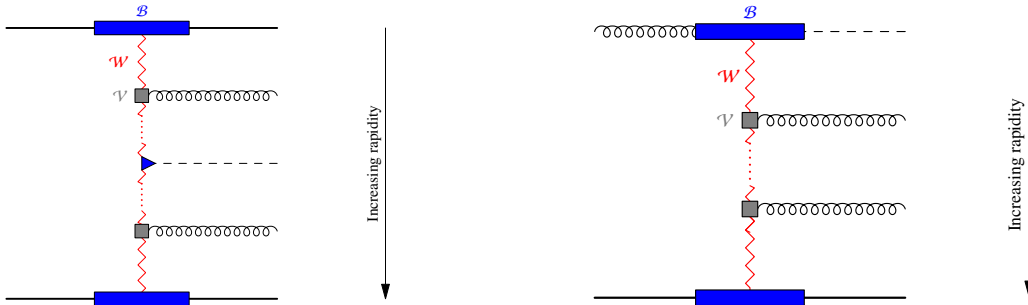
Figure 2: Structure of HEJ matrix elements. The Higgs boson rapidity can be either in between the rapidities of the most backward and the most forward parton (left) or outside this rapidity range (right).

The structure of the LL HEJ matrix elements is illustrated in figure 2. Let us first consider the leading configurations where the Higgs boson is neither the most backward nor the most forward outgoing particle. These configurations first contribute in Higgs boson plus dijet production. According to the criterion introduced in section 2.1, the flavour of the most backward (forward) outgoing particle has to coincide with the flavour f_a (f_b) of the backward (forward) incoming parton. All other outgoing particles apart from the Higgs boson have to be gluons. The all-order

HEJ matrix element has the form

$$
\overline{\left|\mathcal{M}_{\text{HEJ}}^{f_a f_b \to f_a \cdots H \cdots f_b}\right|}^2 = \mathcal{B}_{f_a, H, f_b}(p_a, p_b, p_1, p_n, q_j, q_{j+1})
$$

$$
\cdot \prod_{\substack{i=1 \\ i \neq j}}^{n-2} \mathcal{V}(p_a, p_b, p_1, p_n, q_i, q_{i+1}) \tag{2}
$$

$$
\cdot \prod_{i=1}^{n-1} \mathcal{W}(q_i, y_i, y_{i+1}),
$$

where p_a is the momentum of the backward incoming parton, p_b the momentum of the forward incoming parton, and $q_i = p_a - \sum_{k=1}^{i} p_k$ the ith t-channel momentum. The momentum of the Higgs boson is $p_H \equiv p_j$.

$\mathcal{B}$ denotes the Born-level amplitude. It is given by

$$
\mathcal{B}_{f_a, H, f_b}(p_a, p_b, p_1, p_n, q_j, q_{j+1}) = \frac{1}{4(N_C^2 - 1)} \frac{g_s^2 K_{f_a}(p_1^-, p_a^-)}{t_1} \frac{g_s^2 K_{f_b}(p_n^+, p_b^+)}{t_{n-1}}
$$

$$
\times \frac{1}{t_j t_{j+1}} \sum_{\substack{\lambda_a = +, - \\ \lambda_b = +, -}} \left| j_\mu^{\lambda_a}(p_1, p_a) V_H^{\mu\nu}(q_j, q_{j+1}) j_\nu^{\lambda_b}(p_n, p_b) \right|^2, \tag{3}
$$

where we have introduced the short-hand notation $t_i = q_i^2$. V_H denotes the one-loop Higgs-gluon-gluon vertex, including the full dependence on the top and bottom masses. The colour structure is described by the *colour acceleration modifiers*

$$
K_q = K_{\bar{q}} = C_F,
$$

$$
K_g(p_1^-, p_a^-) = \frac{1}{2} \left(\frac{p_1^-}{p_a^-} + \frac{p_a^-}{p_1^-} \right) \left(C_A - \frac{1}{C_A} \right) + \frac{1}{C_A},
$$

where $C_A = N_C = 3, C_F = \frac{4}{3}$ are the usual colour factors. The final ingredient is the current

$$
j_\mu^\lambda(p, q) = \bar{u}^\lambda(p) \gamma_\mu u^\lambda(q). \tag{4}
$$

In contrast to the Born-level function, the (resolved) real corrections described by $\mathcal{V}$ and the virtual (and unresolved real) correction factors $\mathcal{W}$ are process independent. Up to subtraction terms, they are given by

$$
\mathcal{V}(p_a, p_b, p_1, p_n, q_i, q_{i+1}) = -\frac{C_A g_s^2}{t_i t_{i+1}} V_\mu(p_a, p_b, p_1, p_n, q_i, q_{i+1}) V^\mu(p_a, p_b, p_1, p_n, q_i, q_{i+1}), \tag{5}
$$

$$
V^\mu(p_a, p_b, p_1, p_n, q_i, q_{i+1}) = -(q_i + q_{i+1})^\mu
$$

$$
+ \frac{p_a^\mu}{2} \left(\frac{q_i^2}{p_{i+1} \cdot p_a} + \frac{p_{i+1} \cdot p_b}{p_a \cdot p_b} + \frac{p_{i+1} \cdot p_n}{p_a \cdot p_n} \right) + p_a \leftrightarrow p_1
$$

$$
- \frac{p_b^\mu}{2} \left(\frac{q_{i+1}^2}{p_{i+1} \cdot p_b} + \frac{p_{i+1} \cdot p_a}{p_b \cdot p_a} + \frac{p_{i+1} \cdot p_1}{p_b \cdot p_1} \right) - p_b \leftrightarrow p_n, \tag{6}
$$

$$
\mathcal{W}(q_i, y_i, y_{i+1}) = \exp[(y_i - y_{i+1})\omega^0(q_i)]. \tag{7}
$$

Explicit formulas for the subtraction and for the regularised Regge trajectory ω are given in [12].

Configurations where the Higgs boson is the most backward outgoing particle contribute already in Higgs boson plus single jet production. The `HEJ` amplitude is given by

$$\overline{\left|\mathcal{M}_{\mathrm{HEJ}}^{gf_b \to H \cdots f_b}\right|}^2 = \mathcal{B}_{H,f_b}(p_a, p_b, p_1, p_n)$$
$$\cdot \prod_{i=1}^{n-2} \mathcal{V}(p_a, p_b, p_a, p_n, q_i, q_{i+1}) \tag{8}$$
$$\cdot \prod_{i=1}^{n-1} \mathcal{W}(q_i, y_i, y_{i+1}).$$

The functions $\mathcal{V}$ and $\mathcal{W}$ describing real and virtual corrections are the same as before. The Born-level function for this configuration is [13]

$$\mathcal{B}_{H,f_b} = \frac{1}{4(N_c^2 - 1)} \frac{1}{t_1} \frac{g_s^2 K_{f_b}(p_n^+, p_b^+)}{t_{n-1}} \sum_{\substack{\lambda_a = +,- \\ \lambda_b = +,-}} \left| \epsilon_\mu^{\lambda_a}(p_a) \, V_H^{\mu\nu}(p_a, p_a - p_1) \, j_\nu^{\lambda_b}(p_n, p_b) \right|^2, \tag{9}$$

where $\epsilon^{\lambda_a}(p_a)$ is the polarisation vector of the incoming gluon. The case where the Higgs boson is the most forward emitted particle is completely analogous.

In addition to the leading configurations discussed so far, we also include subleading configurations where either the forward or backward incoming parton is a quark or antiquark, but the corresponding most backward or most forward outgoing particle is a gluon. In this case, the matrix element retains its general structure shown in eqs. (2) and (8), but the Born-level function has to be adjusted for the additional "unordered" emission. For details, see [12].

As illustrated in figure 3, the tree-level truncation of the `HEJ` matrix elements agrees well with the exact results throughout the whole phase space.
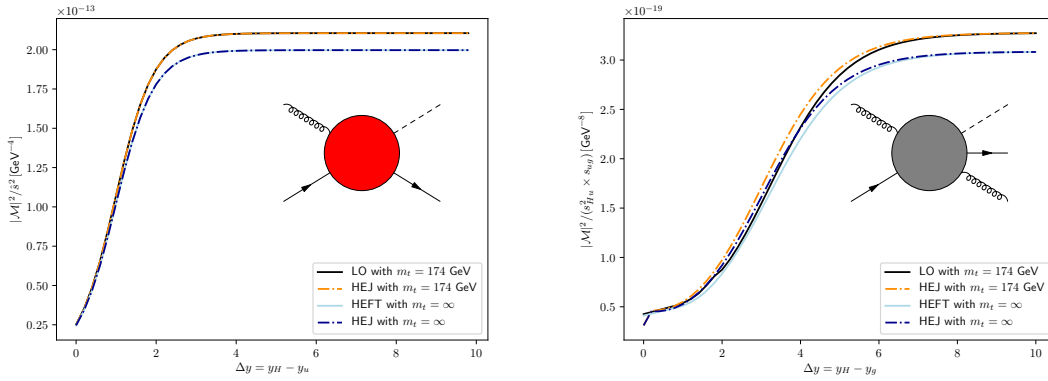
Figure 3: Comparison between exact tree-level matrix elements taken from Madgraph5_aMC@NLO [14] and their `HEJ` approximations.

2.3 Fixed-order matching

To further improve the prediction, we match the `HEJ` prediction to leading order on an event-by-event bases using the method developed in [15]. In this approach, for each input leading-order

event several all-order configurations are generated in a way that preserves the number of jets and their rapidities while slightly shifting transverse momenta. To achieve both leading-order precision and LL resummation, the events are then reweighted such that the final weight is proportional to $\frac{|\mathcal{M}_{\mathrm{LO}}|^2|\mathcal{M}_{\mathrm{HEJ}}|^2}{|\mathcal{M}_{\mathrm{HEJ,\,LO}}|^2}$, where $\mathcal{M}_{\mathrm{LO}}$ is the exact leading-order matrix element and $\mathcal{M}_{\mathrm{HEJ,\,LO}}$ the leading-order truncation of the HEJ matrix element $\mathcal{M}_{\mathrm{HEJ}}$. The leading-order events for Higgs boson production with at most five jets are generated with Sherpa [16] and OpenLoops [17], including the full dependence on the top-quark mass for final states with at most two jets. Note that the HEJ matrix elements account for the full dependence on the bottom- and top-quark mass. We also include final states with more than five jets using the pure HEJ prediction without leading-order matching. Finally, we ensure NLO accuracy for the total cross section via the rescaling

$$\frac{d\sigma}{dO} \to \frac{\sigma_{\mathrm{NLO}}^{m_t \to \infty}}{\sigma_{\mathrm{HEJ}}} \frac{d\sigma}{dO},$$

where $\sigma_{\mathrm{NLO}}^{m_t \to \infty}$ is the total cross section at NLO in the limit of an infinitely heavy top quark and σ_{HEJ} the total HEJ cross section before the rescaling.

3. Results

In figure 4 (taken from [15]), we compare different predictions for the invariant mass spectrum of the two hardest jets in Higgs boson plus dijet production through gluon fusion. Compared to the fixed-order prediction (blue band), we observe a steeper fall-off with increasing invariant mass in the resummed predictions (red and black bands). We also observe an increased effect of finite quark masses (black band) compared to the limit of a massless bottom quark and an infinitely heavy top quark (red band). Together, these effects lower the prediction for the residual cross section after applying weak-boson fusion cuts of $m_{12} > 400 \, \mathrm{Gev}$ and $y_{12} > 2.8$ to 4% of the value before cuts, whereas the fixed-order prediction yields a reduction to 9%.
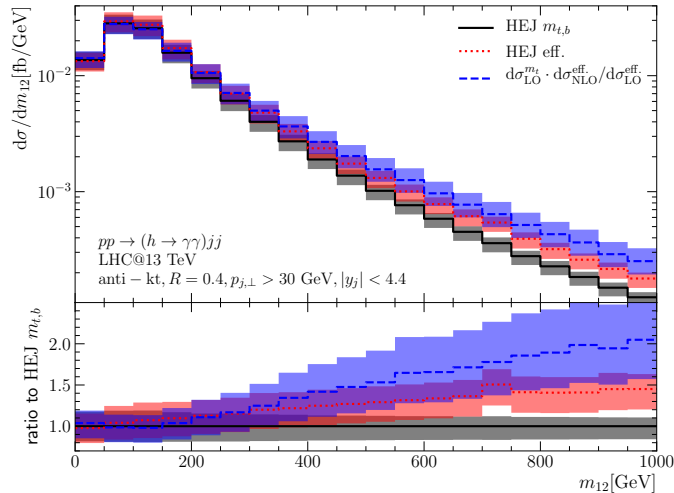
Figure 4: Invariant mass spectrum of the two hardest jets in gluon fusion production of a Higgs boson with at least two jets.

The production of a Higgs boson together with one or more jets within `HEJ` was first considered and compared to experimental data in [13]. In the following, we discuss these results. In the high-energy regime, a similar suppression with respect to fixed order as in [15] was found, cf. figure 5.
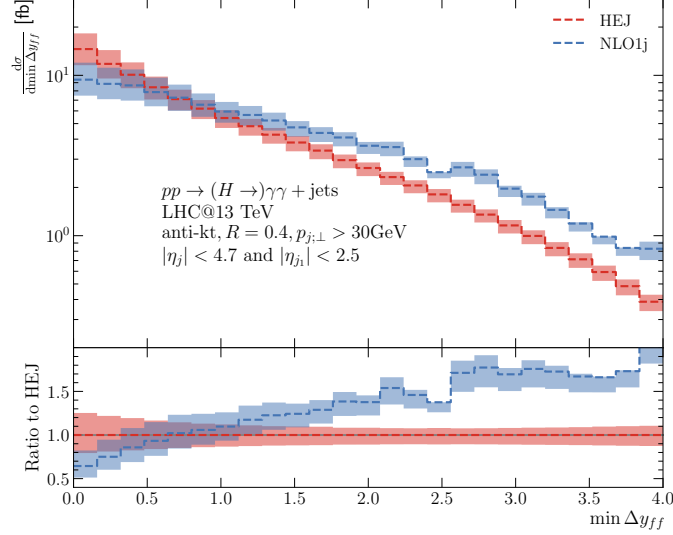
Figure 5: Distribution of the minimum rapidity separation in Higgs boson plus jets production. The `HEJ` prediction (red band) shows a strong suppression compared to the fixed-order prediction (blue band) in the high-energy region of large rapidity differences.

Figure 6 shows a comparison to CMS measurements at 13 TeV [18, 19]. For this comparison, the gluon-fusion predictions have been supplemented with the contributions from other Higgs boson production channels, collectively denoted as "HX". The predictions for those channels were extracted from [18, 19]. `HEJ` predicts a slightly harder transverse momentum spectrum than found at NLO.
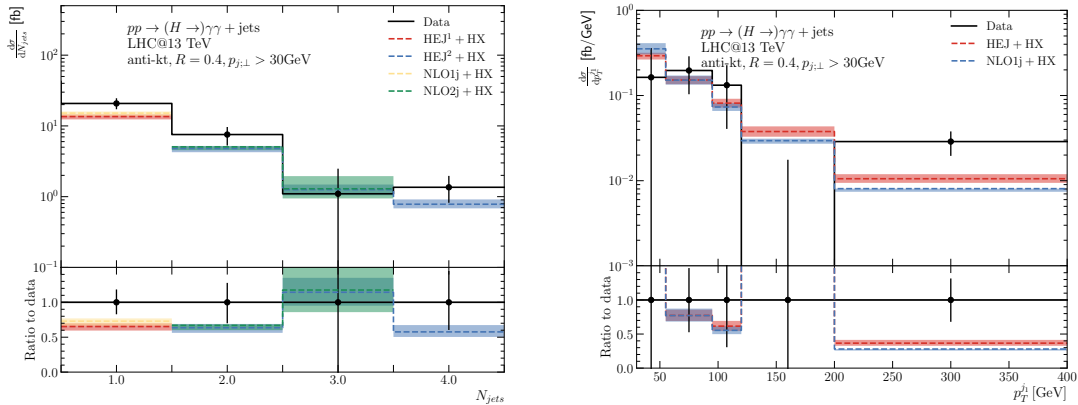
Figure 6: Predictions for the exclusive number of jets (left) and the transverse momentum distribution of the hardest jet (right) for Higgs boson plus jets production compared to CMS measurements [18, 19].

In figure 7, `HEJ` predictions are compared to 8 TeV ATLAS data [20]. Again, we observe

7

a steeper fall-off of the resummed prediction compared to the fixed-order one when approaching the high-energy region of large invariant masses and rapidity separations. This difference is more visible when focusing exclusively on the gluon-fusion contribution, see figure 8.
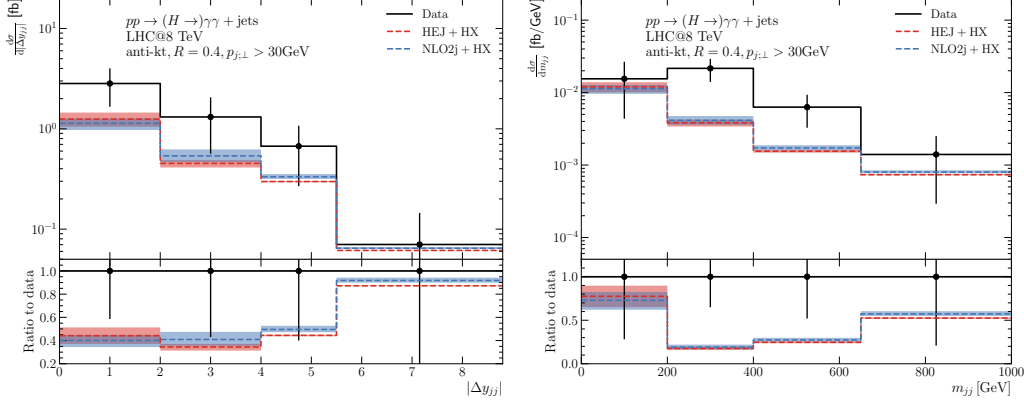
Figure 7: Comparison between theory predictions and ATLAS data [20] for the rapidity separation (left) and the invariant mass (right) between the two hardest jets in Higgs boson plus dijet production.
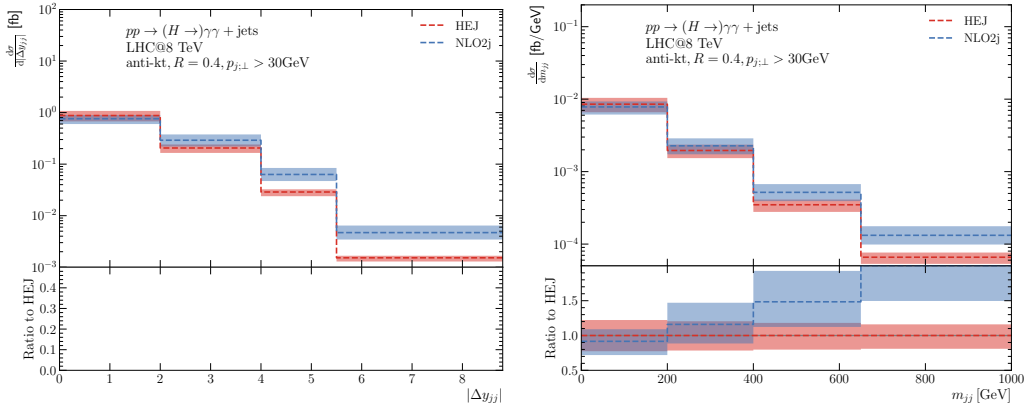
Figure 8: Gluon-fusion contribution to the rapidity separation (left) and the invariant mass (right) between the two hardest jets in Higgs boson plus dijet production.

4. Conclusions

We have shown the first predictions for a process involving a single jet within the *High Energy Jets* framework, obtained in [13]. Compared to fixed-order predictions, we observe a significant suppression in the high-energy region characterised by large invariant masses and large rapidity separations. This feature is particularly important for predicting the gluon-fusion background to weak boson fusion accurately. All-order high-energy resummation for the production of a Higgs boson with at least one jet is implemented in the latest public version 2.2 [21] of the HEJ Monte Carlo event generator.

References

[1] B. Mistlberger, *Higgs boson production at hadron colliders at N^3LO in QCD*, *JHEP* **05** (2018) 028, [1802.00833].

[2] M. Cacciari, F. A. Dreyer, A. Karlberg, G. P. Salam and G. Zanderighi, *Fully Differential Vector-Boson-Fusion Higgs Production at Next-to-Next-to-Leading Order*, *Phys. Rev. Lett.* **115** (2015) 082002, [1506.02660].

[3] J. Cruz-Martinez, T. Gehrmann, E. W. N. Glover and A. Huss, *Second-order QCD effects in Higgs boson production through vector boson fusion*, *Phys. Lett. B* **781** (2018) 672–677, [1802.02445].

[4] F. A. Dreyer and A. Karlberg, *Vector-Boson Fusion Higgs Production at Three Loops in QCD*, *Phys. Rev. Lett.* **117** (2016) 072001, [1606.00840].

[5] T. Liu, K. Melnikov and A. A. Penin, *Nonfactorizable QCD Effects in Higgs Boson Production via Vector Boson Fusion*, *Phys. Rev. Lett.* **123** (2019) 122002, [1906.10899].

[6] M. Ciccolini, A. Denner and S. Dittmaier, *Electroweak and QCD corrections to Higgs production via vector-boson fusion at the LHC*, *Phys. Rev. D* **77** (2008) 013002, [0710.4749].

[7] V. Del Duca, W. Kilgore, C. Oleari, C. Schmidt and D. Zeppenfeld, *Higgs + 2 jets via gluon fusion*, *Phys. Rev. Lett.* **87** (2001) 122001, [hep-ph/0105129].

[8] J. R. Andersen and J. M. Smillie, *Constructing All-Order Corrections to Multi-Jet Rates*, *JHEP* **1001** (2010) 039, [0908.2786].

[9] J. R. Andersen and J. M. Smillie, *The Factorisation of the t-channel Pole in Quark-Gluon Scattering*, *Phys.Rev.* **D81** (2010) 114021, [0910.5113].

[10] J. R. Andersen and J. M. Smillie, *Multiple Jets at the LHC with High Energy Jets*, *JHEP* **1106** (2011) 010, [1101.5394].

[11] V. S. Fadin, R. Fiore, M. G. Kozlov and A. V. Reznichenko, *Proof of the multi-Regge form of QCD amplitudes with gluon exchanges in the NLA*, *Phys. Lett. B* **639** (2006) 74–81, [hep-ph/0602006].

[12] J. R. Andersen, T. Hapola, A. Maier and J. M. Smillie, *Higgs Boson Plus Dijets: Higher Order Corrections*, *JHEP* **09** (2017) 065, [1706.01002].

[13] J. R. Andersen, H. Hassan, A. Maier, J. Paltrinieri, A. Papaefstathiou and J. M. Smillie, *High energy resummed predictions for the production of a Higgs boson with at least one jet*, *JHEP* **03** (2023) 001, [2210.10671].

[14] J. Alwall, R. Frederix, S. Frixione, V. Hirschi, F. Maltoni, O. Mattelaer et al., *The automated computation of tree-level and next-to-leading order differential cross sections, and their matching to parton shower simulations*, *JHEP* **07** (2014) 079, [1405.0301].

PoS(RADCOR2023)090

[15] J. R. Andersen, T. Hapola, M. Heil, A. Maier and J. M. Smillie, *Higgs-boson plus Dijets: Higher-Order Matching for High-Energy Predictions*, *JHEP* **08** (2018) 090, [1805.04446].

[16] Sherpa collaboration, E. Bothmann et al., *Event Generation with Sherpa 2.2*, *SciPost Phys.* **7** (2019) 034, [1905.09127].

[17] F. Buccioni, S. Pozzorini and M. Zoller, *On-the-fly reduction of open loops*, *Eur. Phys. J. C* **78** (2018) 70, [1710.11452].

[18] CMS collaboration, A. M. Sirunyan et al., *Measurement of inclusive and differential Higgs boson production cross sections in the diphoton decay channel in proton-proton collisions at $\sqrt{s}$ = 13 TeV*, *JHEP* **01** (2019) 183, [1807.03825].

[19] CMS collaboration, A. Tumasyan et al., *Measurement of the Higgs boson inclusive and differential fiducial production cross sections in the diphoton decay channel with pp collisions at $\sqrt{s}$ = 13 TeV*, *JHEP* **07** (2023) 091, [2208.12279].

[20] ATLAS collaboration, G. Aad et al., *Measurements of fiducial and differential cross sections for Higgs boson production in the diphoton decay channel at $\sqrt{s}$ = 8 TeV with ATLAS*, *JHEP* **09** (2014) 112, [1407.4222].

[21] J. R. Andersen, B. Ducloué, H. Hassan, C. Elrick, A. Maier, G. Nail et al., *HEJ 2.2: W boson pairs and Higgs boson plus jet production at high energies*, 2303.15778.

PoS(RADCOR2023)090